A Dual-Active Bridge Topology With a Tuned *CLC* Network

Ross P. Twiname, *Member, IEEE*, Duleepa J. Thrimawithana, *Member, IEEE*, Udaya K. Madawala, *Senior Member, IEEE*, and Craig A. Baguley, *Member, IEEE*

***Abstract*—This paper proposes a resonant dual-active bridge (DAB) converter, which uses a tuned capacitor–inductor–capacitor network. In comparison to the conventional DABs, the proposed topology significantly reduces the bridge currents, lowering both conduction and switching losses and improving the bridge power factors. A mathematical model, which predicts the behavior of the proposed system, is presented to show that both the magnitude and direction of the power flow can be controlled through either relative phase angle or pulse width modulation of voltages produced by the bridges. The viability of the proposed concept is verified through simulation. Experimental results of a 4- kW prototype converter, which has an efficiency of 95% at rated power, are also presented with discussions to demonstrate the improved performance of this topology.**

***Index Terms*—DC–DC converter, dual-active bridge (DAB), resonant.**

I. Introduction

GLOBALLY there has been an increased concern in the unsustainable manner in which we meet our electrical energy needs. Concerns lie mainly in the way that we are depleting natural resources such as oil and gas while polluting the environment as we extract energy from these unrenewable sources. This has resulted in electricity increasingly being generated from renewable energy (RE) sources like wind, hydro, tidal, and solar [1]–[4], to address these concerns. Conventionally, large-scale RE generation plants, such as solar and wind farms, have been built and incorporated into the main grid. Efforts to reduce transmission losses have resulted in a shift toward microscale distributed generation (DG) from RE sources [5]–[7]. Power generation through microscale distributed RE sources is highly variable in nature mainly due to the dependence of generation on climate conditions [8]. Some form of energy storage is, therefore, an essential and integral part of most, if not all, RE systems to alleviate the mismatch between electricity supply and demand. Electric vehicles (EVs), which initially emerged as an environmentally friendly and efficient means of transport, can also help to provide power network stability in the presence of these fluctuations when used as vehicle-to-grid (V2G) power sources. EV use in RE systems to supplement energy storage, which is referred to as 'Living & Mobility' [9]–[13], essentially requires a bidirectional power interface between the local grid and the EV battery to allow for charging the battery when surplus energy is being generated and for extracting energy when there is a deficit. To facilitate a V2G connection with the utility grid requires the use of an ac–dc converter stage, known as a "grid inverter," along with a dc–dc converter, which is also required to be bidirectional. The grid inverter is controlled to maintain a constant dc-link voltage either by extracting power from the grid or delivering power to the grid. When the dc–dc converter is delivering power to the load, the grid inverter functions as a rectifier, whereas when the power flow is reversed it works as an inverter generating power at grid frequency [14]–[19].

Of the many converters developed, both wired and wireless options, dual-active bridges (DABs) are gaining popularity as a preferred option for interfacing EVs with the grid [9]–[15], [18], [19]. DABs facilitate bidirectional power transfer with galvanic isolation, have a high power density and can accommodate a wide range of voltages by operating in both buck and boost modes. Early DAB converters were controlled using single-phase-shift (SPS) control to allow for bidirectional power transfer at variable power levels. SPS control, however, leads to a high reactive current in the system, especially when there is an imbalance in voltages. This high reactive current leads to increased conduction losses in the devices decreasing the overall system's efficiency. Various modulation schemes were investigated in [20]–[30] in an effort to reduce the switch current stresses and the attendant switching and conduction losses. These required a more complicated control system than that used with the conventional SPS control.

Various DAB converters employing a form of series resonance have been investigated, some with phase control and fixed frequency [31], [32], and some with frequency control [33], [34]. In a comparison with a fixed-frequency series-resonant DAB variant in [31], the authors concluded that the only advantage of the latter was its lower current distortion, and therefore, reduced eddy-current losses. Also, series resonant DABs typically require a more complex control system, particularly when they are required to operate with wide load and supply voltage variations.

All existing DAB converters fundamentally draw a large reactive current component at full power, and therefore, incur large conduction losses. As a solution, this paper presents a novel

Manuscript received August 15, 2014; revised November 12, 2014; accepted December 10, 2014. Date of publication December 19, 2014; date of current version August 21, 2015. Recommended for publication by Associate Editor D. Vinnikov.

R. P. Twiname and C. A. Baguley are with the Department of Electrical and Electronics Engineering, Auckland University of Technology, Auckland 1010, New Zealand (e-mail: ross.twiname@aut.ac.nz; craig.baguley@aut.ac.nz).

D. J. Thrimawithana and U. K. Madawala are with the Department of Electrical and Computer Engineering, The University of Auckland, Auckland 1010, New Zealand (e-mail: d.thrimawithana@auckland.ac.nz; u.madawala@auckland.ac.nz).

Color versions of one or more of the figures in this paper are available online at http://ieeexplore.ieee.org.

Digital Object Identifier 10.1109/TPEL.2014.2384511

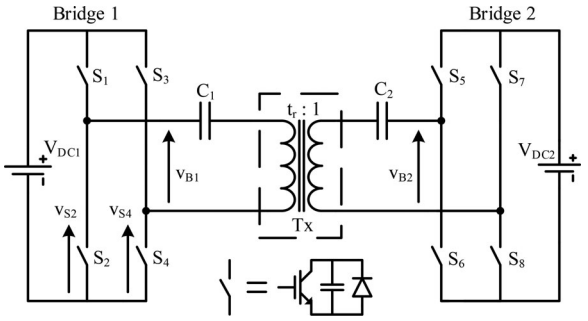

Fig. 1. Proposed resonant DAB converter.

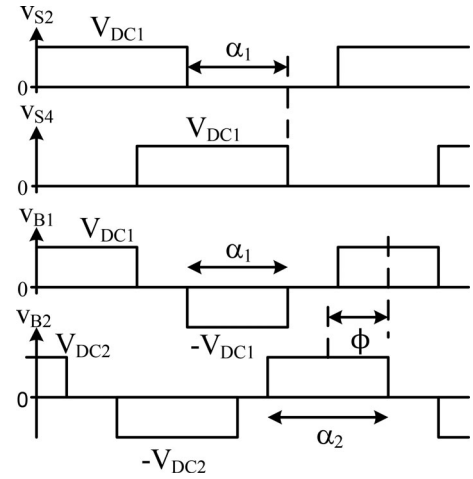

Fig. 2. Bridge voltage waveforms.

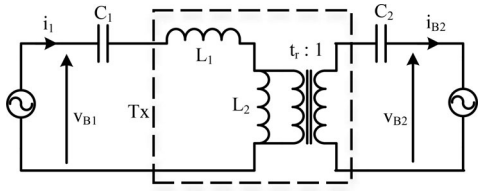

Fig. 3. Initial model.

DAB converter topology, which utilizes a resonant network to minimize the reactive power in the bridges. While the proposed converter is conceptually similar to the *LCL* DAB proposed in [35], including the simple control scheme employed, this variant employs a tuned capacitor–inductor–capacitor (*CLC*) network, which makes use of the magnetizing and leakage inductances of the isolation transformer. In addition, the response of the *CLC* network to harmonic voltages produced by the full-bridge converters is significantly different to that of a DAB employing an *LCL* network. The tuned *CLC* network affects a significant reduction in the magnitude of the bridge currents, and therefore, the switching and copper losses. Equal PWM of each bridge is used to control the magnitude of power flow, while the phase shift between the bridges is fixed at 90° or –90°, according to the direction of power flow required. Theoretical analyses as well as simulated results are presented, together with experimental results obtained from a 4-kW prototype system, to demonstrate the ability of the proposed topology to transfer bidirectional power at a high efficiency for a wide range of dc supply voltages and power.

II. Proposed Resonant DAB

The structure of the proposed resonant DAB (RDAB) converter is shown in Fig. 1. There are two full-bridge converters, each of which operates at a fixed switching-frequency f_s, and outputs a three-level pulse width modulated voltage source from its dc supply. The bridges are coupled with a resonant network comprising C_1, C_2, and transformer *T*x, which also provides galvanic isolation. *T*x has leakage and mutual inductances L_1 and L_2 (see Fig. 3), which are an integral part of the resonant network, which is tuned to the fundamental of the switching frequency, as given by

$$(L_1 + L_2)C_1 = L_2C_2/t_r^2 = \frac{1}{\omega_s^2} = \frac{1}{(2\pi f_s)^2}. \qquad (1)$$

An alternative implementation would use a tightly coupled transformer, having minimal leakage inductance, with a discrete inductor in series with the primary.

Fig. 2 illustrates the switching sequences used to control the RDAB converter's power flow. All bridge switches are operated with 50% duty at the switching frequency f_s, with antiphase switching of the transistors within a leg. A phase displacement α_1 between the legs of Bridge 1 is used to affect PWM of its output voltage V_{B1}, the difference between its leg voltages, as shown in the first three plots. As α_1 changes from 0° to 180° V_{B1}'s duty changes from 0 to 50%, the latter's square waveform corresponding to 100% modulation. V_{B2} is obtained from Bridge 2 in a similar manner, using modulation α_2. The phase-shift ϕ between V_{B1} and V_{B2} determines the direction of the power flow, and is set to either 90° or $-90°$, for forward and reverse operation, respectively.

III. Mathematical Analysis

Analysis of the RDAB converter will be made in the frequency domain under steady-state conditions using a simplified circuit in which there is no resistance. Circuit resistances have a relatively insignificant effect on the currents and will, therefore, be ignored—their losses can be allowed for later. The proposed RDAB of Fig. 1 may initially be modeled by the circuit of Fig. 3, in which the transformer is modeled by an ideal device together with its lumped leakage and mutual inductances, and the two bridges have been modeled as ac voltage sources. In the final Tee network model of Fig. 4, v_1 and v_2 represent v_{B1} and $t_r v_{B2}$, respectively, and C_2 has been relocated to the other side of the ideal transformer, which has then been removed.

A. Circuit Operation at the Fundamental Frequency

In Fig. 4, each of the Tee network's three legs is designed to have the same reactance at the switching (fundamental) frequency

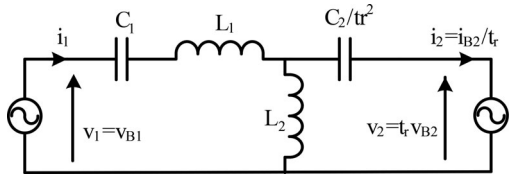

Fig. 4. Model of the RDAB.

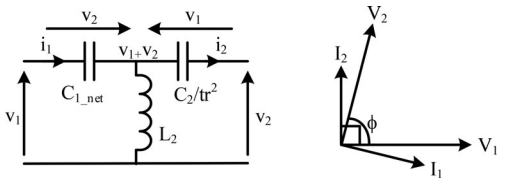

Fig. 5. Fundamental (a) Circuit and (b) Phasors.

$$X_{C1} - X_{L1} = X_{C1\_\text{net}} = X_{L2} = tr^2 X_{C2}. \tag{2}$$

By application of superposition, in which L_2 forms a parallel resonator of infinite reactance with each of the other legs in turn, the central node has a voltage equal to the vector sum of v_1 and v_2. As a result, the voltage across C_1L_1, which behaves as a capacitor C_1_net, is v_2 and the voltage across C_2 is v_1, as shown in Fig. 5(a). In Fig. 5(b), it can be seen that when the converter is operated with ϕ equal to 90° the currents and voltages align so that there is no reactive power, thereby minimizing the bridge currents, which are significantly smaller than those of a conventional DAB converter for which the bridge voltage and current phasors do not align. The same applies for ϕ equal to $-90°$, for power transfer in the opposite direction. To take advantage of this current reduction, and therefore, keep the losses to a minimum, the RDAB is operated with a fixed ϕ of either 90° or $-90°$, for forward and reverse power transfer, respectively. Equal PWM of the bridge voltages with α_1 and α_2 is used to control the magnitude of the power flow. It will be shown in the next section that the fundamental components are dominant in the power calculation, as expected in a resonant system so that the conclusions of the fundamental analysis presented here remain valid.

B. Power Calculation

The voltages generated by the two full-bridge converters can be represented by Fourier series expansions

$$v_1 = \frac{4V_{\text{DC1}}}{\pi} \sum_{n=1,3\ldots}^{\infty} \frac{1}{n} \cos(n\omega_s t) \sin\frac{n\alpha_1}{2} \tag{3}$$

$$v_2 = \frac{4t_r V_{\text{DC2}}}{\pi} \sum_{n=1,3\ldots}^{\infty} \frac{1}{n} \cos(n\omega_s t + n\phi) \sin\frac{n\alpha_2}{2}. \tag{4}$$

A specific frequency component of v_1, the nth harmonic, has a phasor V_1 whose rms representation is given by

$$V_1(n\omega_s) = \frac{4V_{\text{DC1}}}{n\pi\sqrt{2}} \sin\frac{n\alpha_1}{2}. \tag{5}$$

Similarly, v_2 is represented by a phasor V_2

$$V_2(n\omega_s) = \frac{4t_r V_{\text{DC2}}}{n\pi\sqrt{2}} \sin\frac{n\alpha_2}{2}(\cos n\phi + j\sin n\phi). \tag{6}$$

At f_s the reactance of the L_1C_1 leg is equal to $X_{C1} - X_{L1}$, and is equal to the reactance of each of the other two legs. There is, therefore, a degree of freedom in the choice of L_1, which may, along with the other components, be specified in terms of a design base reactance value, X_B at f_s

$$\begin{aligned} X_{L1} &= k_1 X_B \\ X_{C1} &= (1+k_1) X_B \\ X_{L2} &= X_{C2} = X_B. \end{aligned} \tag{7}$$

For these parameters, the corresponding i_1 and i_2 current phasors, I_1 and I_2, are given by (8) and (9), respectively

$$I_1 = \frac{j(n^3(V_1 - V_2) - nV_1)}{X_B((2n^2-1)(1+k_1) - n^4 k_1)} \tag{8}$$

$$I_2 = \frac{j(nk_2V_2 - n^3(k_1V_2 + k_3(V_2 - V_1)))}{X_B((2n^2-1)(1+k_1) - n^4 k_1)}. \tag{9}$$

The power transfer is calculated by evaluating the real part of the product of V_1 and I_1 (or V_2 and I_2) after substitution of (5)–(7) into (8) and (9), extracting products of similar frequency components, and is given by

$$\begin{aligned} P &= \sum \text{Re}(V_1 I_1) = \sum \text{Re}(V_2 I_2) \\ &= P_B \sum_{n=1,3\ldots} \frac{n\sin\left(\frac{n\alpha_1}{2}\right)\sin\left(\frac{n\alpha_2}{2}\right)\sin n\phi}{((2n^2-1)(1+k_1) - n^4 k_1)} \end{aligned} \tag{10}$$

where

$$P_B = \frac{8t_r V_{\text{DC1}} V_{\text{DC2}}}{\pi^2 X_B}. \tag{11}$$

In (10), the magnitude of the power flowing from V_{DC1} to V_{DC2} can be controlled by modulating the magnitudes of v_1 and v_2 with α_1 and α_2, and the direction controlled by setting ϕ to either $+90°$, for positive P values, or $-90°$ for negative P values. In this form, the base power P_B will have its normalized value of $8/\pi^2 \approx 0.8106$ for equal weighted dc supply voltages V_{DC1} and $t_r V_{\text{DC2}}$ of 1 V, and for an X_B value of 1 Ω. For equal bridge modulations α_1 and α_2, the summation term in (10) is approximately a sine squared function of modulation whose only significant harmonic component is the third harmonic, the magnitude of which depends on the value of parameter k_1. Small values of k_1 result in an increase in the bridge currents, and to a lesser extent the power, as the third-harmonic component is accentuated. This effect is greatest for relative modulations of 1/3, for which this component is largest, as shown in Fig. 6 for a converter operated with $\phi = 90°$ and equal bridge modulations. Conversely, it can be seen that the third harmonic has no effect at a relative modulation of 2/3, for which there is a Fourier series null. Series resonance causes a pole in the denominator of (8)–(10) at $k_1 = 17/64 \approx 0.27$, placing a lower limit on the value of k_1, the relative value of the series inductor L_1.

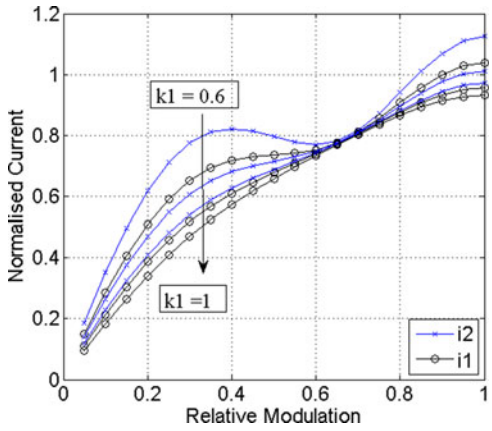

Fig. 6. Effect of relative L_1 value.

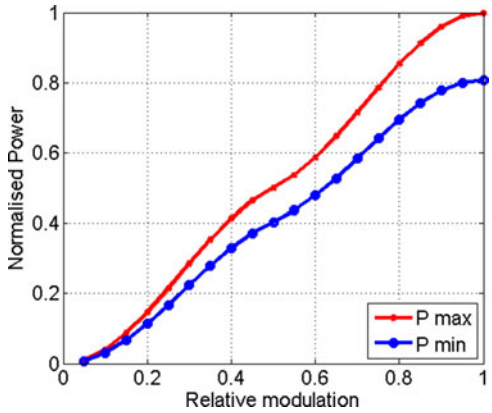

Fig. 7. Power sensitivity to component variations for $k_1 = 0.6$.

Fig. 7 shows the converter's normalized power range when operated with $\phi = 90°$ and with equal bridge modulations. To gauge the power sensitivity of the converter, (10) was evaluated for Monte-Carlo variations of $\pm 10\%$ in the value of each of the four reactive elements. From this, it can be seen that the converter's power is not very sensitive to component variations. The third-harmonic component of the currents causes the local rise in the power curve at a relative modulation of 1/3, but its effect is relatively small compared to the current variations seen in Fig. 6.

A key feature of this RDAB converter is its reduced full-power bridge current values, by virtue of near-zero reactive currents. Table I provides a more complete comparison with a DAB converter using SPS modulation, for two power levels and for two dcr values, as given by

$$\mathrm{dcr} = t_r \frac{V_{\mathrm{DC2}}}{V_{\mathrm{DC1}}}. \tag{12}$$

Two sets of RDAB results are shown, with different k_1 values, along with results for two SPS converters, designed for maximum modulation phase shifts of 0.5 π (90°) and 0.35 π (63°). The full-power RDAB bridge current values shown, the average for the two bridges, are smaller than those of the SPS DAB, particularly for nonunity dcr values and for the SPS converter

TABLE I
COMPARISON OF RDAB CONVERTER WITH SPS DAB CONVERTER

Converter Type	dcr	I_{Bridge} (A)		Efficiency (%)	
		4 kW	400 W	4 kW	400 W
RDAB $k_1 = 0.6$	1	12	5.2	94.1	77.8
	2	13	6.2	92.7	69.3
RDAB $k_1 = 1$	1	11.2	4	95.3	83.2
	2	12.3	4.8	94.4	76.5
SPS $\phi_{\mathrm{max}} = 90°$	1	16.4	1	90.7	96.3
	2	22.9	8.3	88.6	61.3
SPS $\phi_{\mathrm{max}} = 63°$	1	13.5	1	92.7	96.3
	2	16.2	9.1	90.8	57.9

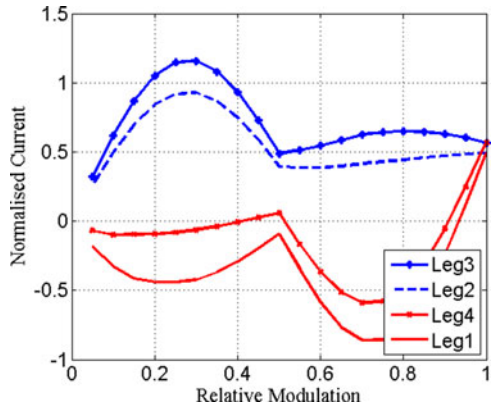

Fig. 8. Minimum leg currents at the switching points.

operating in the full 90° range. At 10% of the maximum design power, the RDAB has smaller bridge current values when the bridge dc voltages are unbalanced. Expressions for the rms values of the RDAB bridge currents are included in Appendix A. Although the values shown in the table are dependent on many parameters, they should serve as a useful comparison of the converters, as they were calculated for systems having identical IGBT bridges and which were similar in other respects. The efficiency values, although likely to be slightly larger than those to be gained experimentally, are reasonably indicative of the trends.

C. Zero-Voltage Switching Range

Zero-voltage switching (ZVS) will be deemed to occur for a transistor, which is being gated on while carrying a reverse current through its antiparallel diode—the energy required to swing the output capacitor's voltage to the other rail [36] will be ignored. Unlike a conventional DAB converter, the RDAB converter is almost unaffected by changes in the dc voltage conversion ratio. The ZVS status of each of the four bridge legs is determined by evaluating the switching currents of the transistors in those legs. Equal bridge modulations were used for the tests, with Bridge 2 leading Bridge 1 by 90° and with a k_1 value of 0.6. Fig. 8 shows the minimum or worst-case switching current values which occur in each leg for a variation in dcr from 0.7 to 1.4 and for $\pm$ 10% Monte-Carlo component

TABLE II
PARAMETERS OF THE RDAB CONVERTER

Parameter	Design Value	Experimental Value
Rated Power	4286 W	
V_{DC1}	400 V	
V_{DC2}	400 V	
Switches	STGWA19N60 IGBT	
f_s	50 kHz	
X_B	31.83 Ω	
C_1	48.46 nF	48.6 nF
C_2	100 nF	100.2 nF
Transformer	Dual TDG E65 cores, TP4 ferrite	
	Primary 7080 V.μs, 11.7 Arms	
	Secondary 4340 V.μs, 12.1 A rms	
L_1	107.8 μH	100.9 μH
L_2	101.3 μH	105.6 μH

TABLE III
AC RESISTANCES OF THE NETWORK

f (kHz)	50	150	250	350	450	550
R_1 (Ω)	0.076	0.281	0.765	1.440	2.241	3.062
R_2 (Ω)	0.115	0.456	1.005	1.841	3.104	4.867

variations. For the chosen current directions, a positive current value indicates ZVS. From the figure, it is seen that the leading leg of the leading bridge (Leg 3, switches S_5 and S_6) and the lagging leg of the lagging bridge (Leg 2, switches S_3 and S_4) have ZVS under all conditions, while the other two legs only achieve ZVS at maximum modulation.

IV. RESULTS

A 4-kW RDAB converter having the parameters given in Table II has been designed and tested to validate the model and the mathematical analysis. Simulation and experimental results are presented here for a range of modulation levels and for forward and reverse power transfers. Simulations were performed with MATLAB in the frequency domain so that the frequency-dependent resistances shown in Table III would be included in the calculations. R_1 and R_2 are the effective resistances at the bridge ports, that is they appear in series with C_1 and C_2 in Fig. 4. In the converter which was built, with the values specified in Table II, a loosely coupled transformer was used to implement L_1 as its leakage inductance and L_2 as its mutual inductance. Metalized polypropylene capacitors were used for C_1 and C_2. Control of the bridges was from a fixed gate driver, which generated bridge voltages with equal modulations and with an angle between them of either 90° or −90°, to suite the direction of power transfer. A fixed dead band of 350 ns was used in each leg to prevent cross-current conduction.

Initial tests were conducted with each side of the converter connected to a 400-V dc source. The simulated voltages and currents of the proposed system when transferring rated power in the forward direction are shown in Fig. 9. Here, both bridges have the maximum α_1 and α_2 values of 180°, and Bridge 2 leads Bridge 1 by 90°. The experimentally obtained waveforms

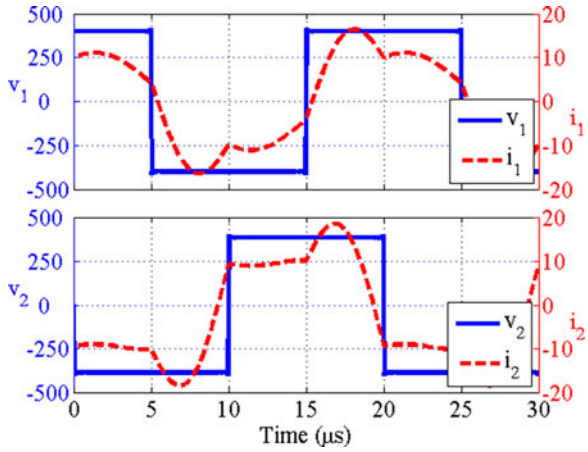

Fig. 9. Simulated voltage and current waveforms for 100% forward modulation.

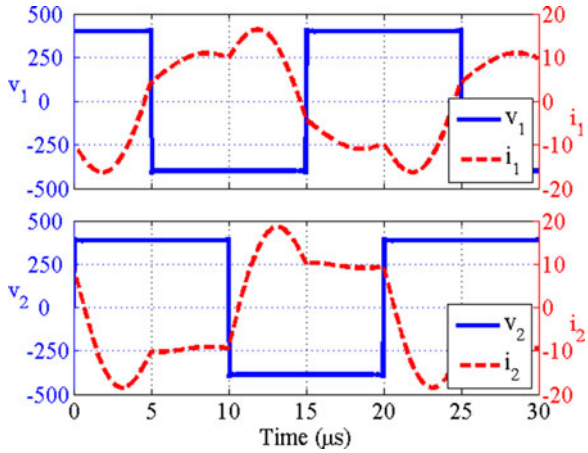

Fig. 10. Simulated voltage and current waveforms for 100% reverse modulation.

were indistinguishable from those of the simulation, and therefore, have not been shown separately. The bridge currents are approximately sinusoidal and in phase with their respective voltages, indicating a near zero reactive power transfer between the bridges and the *CLC* resonant network, as predicted by the theory.

Fig. 10 shows the waveforms obtained through simulation when the DAB is transferring rated power in the reverse direction, with Bridge 1 leading Bridge 2 by 90°, in accordance with (9). Again, the experimentally obtained waveforms were indistinguishable from those of the simulation. The magnitude and the shape of the bridge currents are similar to those in Fig. 9, but are in antiphase with respect to their corresponding bridge voltages, as expected for reverse power transfer. Fig. 11 shows the reverse power transfer of approximately 3 kW obtained when α_1 and α_2 are reduced to give 70% modulation while maintaining ϕ at −90°. The experimental waveforms closely match those calculated theoretically. Again the bridge voltages and currents are in antiphase indicating minimal reactive power transfer between the bridges and the *CLC* resonant network. Also noticeable is how strongly the current waveforms resemble sinusoids—the

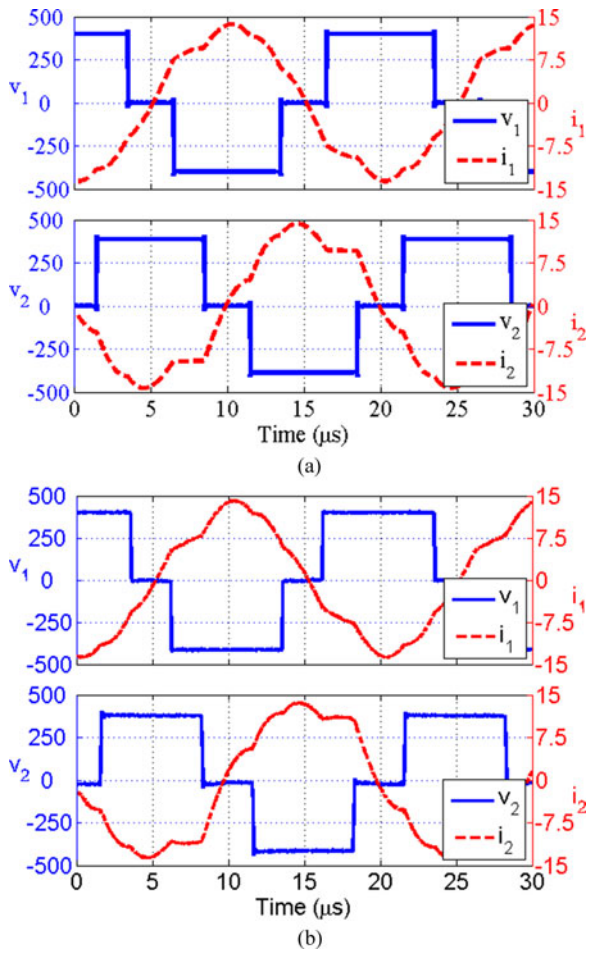

Fig. 11. (a) Simulated and (b) experimental voltage and current waveforms for 70% reverse modulation.

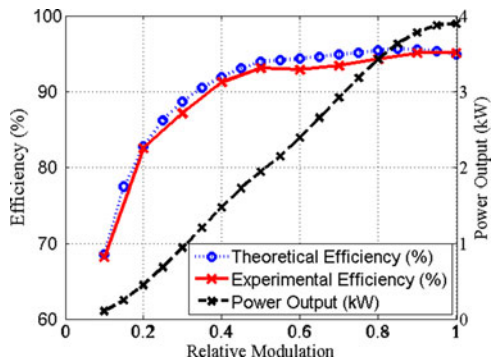

Fig. 12. Efficiency and power transfer of the prototype RDAB converter for forward operation with $V_{\mathrm{DC1}} = V_{\mathrm{DC2}} = 400$ V.

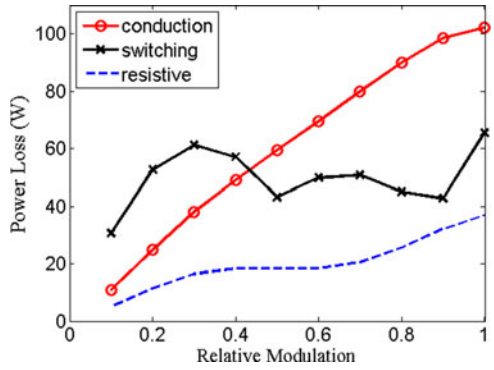

Fig. 13. Calculated losses of the prototype RDAB converter for forward operation with $V_{\mathrm{DC1}} = V_{\mathrm{DC2}} = 400$ V.

modulation is close to the value of 2/3, which results in a null in the third harmonic.

Fig. 12 shows the efficiency of the converter for a range of forward power transfers. The experimental values track the theoretical values quite closely—the theoretical calculations do not take into account the dynamic aspects of the IGBT switching losses [37], [38], nor the 350-ns conduction dead band between devices in a leg. Furthermore, the system efficiency is maintained at a high level for a wide range of power, dropping steeply to 68% at a power output of 70 W. In Fig. 13 plot of calculated losses, the resistance and conduction losses increase with power [39], as expected. Variations in the third-harmonic component, as seen in Fig. 6, cause the waver in the resistive loss line. The resistive losses, which are largely attributable to the transformer, are higher than normal on account of the transformer construction: To achieve the required leakage inductance in the prototype version, the two sets of windings had a large separation, thereby limiting the window size for the windings, and therefore, the wire gauge—a purpose-built magnetic shunt would be an improvement. The switching losses, although varying with modulation, are not correlated with the power output. They match the "two bump" shape of Fig. 8, except for their rise in the interval above 90% modulation, which is attributable to ZVS being gained in legs 1 and 4, and the attendant loss of zero-current switching at turn-off. The IGBTs that were used had a turn-off loss of approximately twice their turn-on loss. For reverse operation, the efficiency curves are almost identical to those of Fig. 12

$$\bar{I}_1 = \frac{4}{\pi X_B \sqrt{2}} \sqrt{\sum_{n=1,3\ldots} \left(\frac{\left(n^2 t_r V_{\mathrm{dc2}} \sin\frac{n\alpha_2}{2} \sin n\phi\right)^2 + \left((n^2-1)V_{\mathrm{dc1}} \sin\frac{n\alpha_1}{2} - n^2 t_r V_{\mathrm{dc2}} \sin\frac{n\alpha_2}{2} \cos n\phi\right)^2}{((2n^2-1)(1+k_1) - n^4 k_1))^2} \right)}$$

$$\bar{I}_2 = \frac{4}{\pi X_B \sqrt{2}} \sqrt{\sum_{n=1,3\ldots} \left(\frac{\left((n^2-1)(1+k_1) t_r V_{\mathrm{dc2}} \sin\frac{n\alpha_2}{2} \sin n\phi\right)^2 + \left(n^2 V_{\mathrm{dc1}} \sin\frac{n\alpha_1}{2} - (n^2-1)(1+k_1) t_r V_{\mathrm{dc2}} \sin\frac{n\alpha_2}{2} \cos n\phi\right)^2}{((2n^2-1)(1+k_1) - n^4 k_1))^2} \right)}.$$

TABLE IV
EFFICIENCY VARIATION WITH OUTPUT POWER

$V_{DC1} = 300$ V, $V_{DC2} = 400$ V				
Forward				
Modulation (%)	10	30	70	100
Power (W)	47	610	2136	2860
Efficiency (%)	62.6	86.2	93.7	94.4
Reverse				
Modulation (%)	10	30	70	100
Power (W)	74	765	2166	2931
Efficiency (%)	72.9	89.0	93.8	94.3

for forward operation. Similarly, the reverse operation losses are almost identical to those of Fig. 13 for forward operation.

Thus far, the results presented are for a converter operating with matched loads, that is $\mathrm{dcr} = 1$. It has been stated that the efficiency of the RDAB converter is almost unaffected by changes in the dc voltage conversion ratio. This is borne out by the experimental results recorded in Table IV, in which the conversion efficiency obtained at dcr values of 1.33 and 0.75 is approximately the same as those for $V_{DC1} = V_{DC2} = 400$ V. The only significant effect of a reduced dc voltage is the reduced maximum power output.

V. CONCLUSION

A novel DAB topology that employs a *CLC* resonant network has been described. The mathematical model presented has been shown to accurately predict the performance of the proposed topology. Although, the RDAB presented in this paper has not been optimized for efficiency, the results of a 4-kW prototype operated under various conditions suggest a significant improvement in performance in comparison to a conventional DAB converter with SPS control. The lower bridge currents of the resonant DAB topology result in an increased power capacity and a higher efficiency over a wide range of bridge dc supply voltages. In comparison with the conventional converter's hardware, the RDAB converter requires the addition of two relatively low-cost capacitors and for these to be tuned with the transformer. As a bonus, these capacitors provide dc current reset, preventing core saturation in the event of abnormal operating conditions. In regard to tuning, it has been shown that the converter's operating characteristics are not particularly sensitive to variations in the component values. There is the potential to further increase the operating efficiency by employing a purpose-designed transformer employing a magnetic shunt to affect the required leakage inductance. This transformer will be smaller than that of a conventional DAB converter on account of the lower operating currents.

APPENDIX A
NETWORK RMS CURRENT VALUES

Please see the equations at the bottom of the previous page.

REFERENCES

[1] M. H. Nehir, C. Wang, and S. R. Guda, "Alternative energy distributed generation: Need for multi-source operation," in *Proc. North Amer. Power Symp.*, 2006, pp. 547–551.

[2] T. J. Hammons, J. C. Boyer, S. R. Conners, M. Davies, M. Ellis, M. Fraser, E. Holt, and J. Markard, "Renewable energy alternatives for developed countries," *IEEE Trans. Energy Convers.*, vol. 15, no. 4, pp. 481–493, Dec. 2000.

[3] P. K. Katti and M. K. Khedkar, "Fostering the use of low impact renewable energy technologies with integrated operation is the key for sustainable energy system," in *Proc. Joint Int. Conf. Power Syst. Technol. IEEE Power India*, 2008, pp. 1–8.

[4] J. L. Sawin. (2014, Aug. 13). *Renewables 2013 - Global Status Report*. [Online]. Available: http://www.ren21.net/portals/0/documents/resources/gsr/2013/gsr2013_lowres.pdf

[5] U. K. Madawala, D. J. Thrimawithana, X. Dai, and D. M. Vilathgamuwa, "A model for a multi-sourced green energy system," in *Proc. IEEE Conf. Sustainable Energy Technol.*, 2010, pp. 1–6.

[6] J. Marsden, "Distributed generation systems: A new paradigm for sustainable energy," in *Proc. IEEE Green Technol.*, 2011, pp. 1–4.

[7] R. Ramakumar and P. Chiradeja, "Distributed generation and renewable energy systems," in *Proc. 37th Intersoc. Energy Convers. Eng. Conf.* , 2002, pp. 716–724.

[8] S. I. Mustapa, Y. P. Leong, and A. H. Hashim, "Issues and challenges of renewable energy development: A Malaysian experience," in *Proc. Int. Conf. Energy Sustainable Develop.: Issues Strategies*, 2010, pp. 1–6.

[9] W. Kempton and S. Letendre, "Electric vehicles as a new power source for electric utilities," *Transp. Res. Part D, Transport Environ.*, vol. 2, pp. 157–175, 1997.

[10] B. Kramer, S. Chakraborty, and B. Kroposki, "A review of plug-in vehicles and vehicle-to-grid capability," in *Proc. IEEE Ind. Electron.*, 2008, pp. 2278–2283.

[11] U. K. Madawala, P. Schweizer, and V. V. Haerri, ""Living and mobility"—A novel multipurpose in-house grid interface with plug-in hybrid blue angel," in *Proc. IEEE Conf. Sustainable Energy Technol.*, 2008, pp. 531–536.

[12] U. K. Madawala and D. J. Thrimawithana, "A bidirectional inductive power interface for electric vehicles in V2G systems," *IEEE Trans. Ind. Electron.*, vol. 58, no. 10, pp. 4789–4796, Oct.2011.

[13] D. J. Thrimawithana, U. K. Madawala, R. Twiname, and D. M. Vilathgamuwa, "A novel matrix converter based resonant dual active bridge for V2G applications," in *Proc. IPEC Conf. Power Energy*, 2012, pp. 503–508.

[14] D. C. Erb, O. C. Onar, and A. Khaligh, "An integrated bi-directional power electronic converter with multi-level AC-DC/DC-AC converter and non-inverted buck-boost converter for PHEVs with minimal grid level disruptions," in *Proc. IEEE Vehicle Power Propulsion Conf.*, 2010, pp. 1–6.

[15] R. L. Steigerwald, R. W. De Doncker, and H. Kheraluwala, "A comparison of high-power DC-DC soft-switched converter topologies," *IEEE Trans. Ind. Appl.*, vol. 32, no. 5, pp. 1139–1145, Sep./Oct. 1996.

[16] J. Walter and R. W. De Doncker, "High-power galvanically isolated DC/DC converter topology for future automobiles," in *Proc. IEEE 34th Annu. Power Electron. Spec. Conf.*, 2003, vol. 1, pp. 27–32.

[17] N. D. Weise, K. Basu, and N. Mohan, "Advanced modulation strategy for a three-phase AC-DC dual active bridge for V2G," in *Proc. IEEE Vehicle Power Propulsion Conf.*, 2011, pp. 1–6.

[18] N. D. Weise, K. K. Mohapatra, and N. Mohan, "Universal utility interface for plug-in hybrid electric vehicles with vehicle-to-grid functionality," in *Proc. IEEE Power Energy Soc. Gen. Meeting*, 2010, pp. 1–8.

[19] D. Yu, S. Lukic, B. Jacobson, and A. Huang, "Review of high power isolated bi-directional DC-DC converters for PHEV/EV DC charging infrastructure," in *Proc. IEEE Energy Convers. Congr. Expo.*, 2011, pp. 553–560.

[20] Z. Biao, S. Qiang, L. Wenhua, and S. Weixin, "Current-stress-optimized switching strategy of isolated bidirectional DC-DC converter with dual-phase-shift control," *IEEE Trans. Ind. Electron.*, vol. 60, no. 10, pp. 4458–4467, Oct. 2013.

[21] Z. Biao, Y. Qingguang, and S. Weixin, "Extended-phase-shift control of isolated bidirectional DC-DC converter for power distribution in microgrid," *IEEE Trans. Power Electron.*, vol. 27, no. 11, pp. 4667–4680, Nov. 2012.

[22] B. Hua, N. Ziling, and C. C. Mi, "Experimental comparison of traditional phase-shift, dual-phase-shift, and model-based control of isolated bidirectional DC-DC converters," *IEEE Trans. Power Electron.*, vol. 25, no. 6, pp. 1444–1449, Jun. 2010.
[23] A. K. Jain and R. Ayyanar, "PWM control of dual active bridge: Comprehensive analysis and experimental verification," *IEEE Trans. Power Electron.*, vol. 26, no. 4, pp. 1215–1227, Apr. 2011.
[24] F. Krismer and J. W. Kolar, "Closed form solution for minimum conduction loss modulation of DAB converters," *IEEE Trans. Power Electron.*, vol. 27, no. 1, pp. 174–188, Jan. 2012.
[25] F. Krismer and J. W. Kolar, "Efficiency-optimized high-current dual active bridge converter for automotive applications," *IEEE Trans. Ind. Electron.*, vol. 59, no. 7, pp. 2745–2760, Jul. 2012.
[26] F. Krismer, S. Round, and J. W. Kolar, "Performance optimization of a high current dual active bridge with a wide operating voltage range," in *Proc. 37th IEEE Power Electron. Spec. Conf.*, 2006, pp. 1–7.
[27] K. Myoungho, M. Rosekeit, S. Seung-Ki, and R. W. A. A. De Doncker, "A dual-phase-shift control strategy for dual-active-bridge DC-DC converter in wide voltage range," in *Proc. IEEE 8th Int. Conf Power Electron. ECCE Asia*, 2011, pp. 364–371.
[28] G. G. Oggier, G. O. Garci, and A. R. Oliva, "Modulation strategy to operate the dual active bridge DC-DC converter under soft switching in the whole operating range," *IEEE Trans. Power Electron.*, vol. 26, no. 4, pp. 1228–1236, Apr. 2011.
[29] G. G. Oggier, R. Ledhold, G. O. Garcia, A. R. Oliva, J. C. Balda, and F. Barlow, "Extending the ZVS operating range of dual active bridge high-power DC-DC converters," in *Proc. 37th IEEE Power Electron. Spec. Conf.*, 2006, pp. 1–7.
[30] B. Zhao, Q. Song, and W. Liu, "Efficiency characterization and optimization of isolated bidirectional DC-DC converter based on dual-phase-shift control for DC distribution application," *IEEE Trans. Power Electron.*, vol. 28, no. 4, pp. 1711–1727, Apr. 2013.
[31] R. Lenke, F. Mura, and R. W. A. De Doncker, "Comparison of non-resonant and super-resonant dual-active ZVS-operated high-power DC-DC converters," in *Proc. IEEE Power Electron. Appl.*, 2009, pp. 1–10.
[32] L. Xiaodong and A. K. S. Bhat, "Analysis and design of high-frequency isolated dual-bridge series resonant DC/DC converter," *IEEE Trans. Power Electron.*, vol. 25, no. 4, pp. 850–862, Apr. 2010.
[33] Z. Pavlovic, J. A. Oliver, P. Alou, O. Garcia, and J. A. Cobos, "Bidirectional dual active bridge series resonant converter with pulse modulation," in *Proc. 27th Annu. IEEE Appl. Power Electron. Conf. Expo.*, 2012, pp. 503–508.
[34] C. Wei, R. Ping, and L. Zhengyu, "Snubberless bidirectional DC-DC converter with new CLLC resonant tank featuring minimized switching loss," *IEEE Trans. Ind. Electron.*, vol. 57, no. 9, pp. 3075–3086, Sep. 2010.
[35] R. P. Twiname, D. J. Thrimawithana, U. K. Madawala, and C. A. Baguley, "A new resonant bidirectional DC-DC converter topology," *IEEE Trans. Power Electron.*, vol. 29, no. 9, pp. 4733–4740, Sep. 2014.
[36] M. N. Kheraluwala, R. W. Gascoigne, D. M. Divan, and E. D. Baumann, "Performance characterisation of a high-power dual active bridge DC-to-DC converter," *IEEE Trans. Ind. Appl.*, vol. 28, no. 6, pp. 1294–1301, Nov./Dec. 1992.
[37] G. Ortiz, H. Uemura, D. Bortis, J. W. Kolar, and O. Apeldoorn, "Modeling of soft-switching losses of IGBTs in high-power high-efficiency dual-active-bridge DC/DC converters," *IEEE Trans. Electron Devices*, vol. 60, no. 2, pp. 587–597, Feb. 2013.
[38] P. Ranstad and H. P. Nee, "On dynamic effects influencing IGBT losses in soft-switching converters," *IEEE Trans. Power Electron.*, vol. 26, no. 1, pp. 260–271, Jan. 2011.
[39] J. W. Kolar, F. Krismer, Y. Lobsiger, J. Muhlethaler, T. Nussbaumer, and J. Minibock, "Extreme efficiency power electronics," in *Proc. 7th Int. Conf. Integr. Power Electron. Syst.* , 2012, pp. 1–22.

Ross P. Twiname (M'06) received the B.E. degree in electrical engineering from The University of Auckland, Auckland, New Zealand, in 1975.

After a number of years in the industry, he joined the Department of Electrical and Electronic Engineering, Auckland University of Technology, where he presently is a Senior Lecturer. His research interests include electronic applications and power conversion.

Duleepa J. Thrimawithana (M'09) received the B.E. degree (with first-class Hons.) in electrical engineering and the Ph.D. degree in power electronics from The University of Auckland, Auckland, New Zealand, in 2005 and 2009, respectively.

From 2005 to 2008, he worked, in collaboration with Tru-Test Ltd., Manukau, New Zealand, as a Research Engineer in the areas of power converters and high-voltage pulse generator design. In 2008, he joined the Department of Electrical and Computer Engineering, The University of Auckland, as a part-time Lecturer, where he is currently working as a Senior Lecturer in the same department. His main research areas include the fields of inductive power transfer, power electronics and renewable energy.

Dr. Thrimawithana serves as the Chairman of the Joint Chapter of IEEE Industrial Electronics Society and IEEE Industrial Applications Society in New Zealand (north).

Udaya K. Madawala (M'95–SM'06) received the B. Sc. (electrical engineering) (Hons.) degree from The University of Moratuwa, Moratuwa, Sri Lanka, in 1987, and the Ph.D. (power electronics) degree from The University of Auckland, Auckland, New Zealand, in 1993.

After working in industry, he joined the Department of Electrical and Computer Engineering, The University of Auckland as a Research Fellow in 1997, where he is currently an Associate Professor. His research interests include the fields of power electronics, inductive power transfer, and renewable energy.

Dr. Madawala is an active IEEE volunteer and serves as an Associate Editor for the IEEE TRANSACTIONS ON INDUSTRIAL ELECTRONICS and the IEEE TRANSACTIONS ON POWER ELECTRONICS. He is a Member of the Power Electronics Technical Committee of Industrial Electronics Society and the Sustainable Energy Systems Committee of the IEEE Power Electronics Society.

Craig A. Baguley (M'11) received the Ph.D. degree from the University of Auckland, Auckland, New Zealand, in 2011.

He is currently with the Auckland University of Technology, Auckland. His research interests include high-voltage pulse transformer design, high-frequency induction heating, electrical muscle stimulation techniques, and high current power supply design.